



Journal of Geophysical Research: Atmospheres

RESEARCH ARTICLE

10.1002/2017JD027990

Key Points:

- Continual radio frequency is a collection of short duration impulses (less than 160 ns) occurring in explosive eruptions
- Continual radio frequency occurred before charge separation was detected in the eruption column implying that the charge was initially well mixed
- Continual radio frequency impulses likely result from small (less than 10 m) streamer discharges in the jet phase of the eruption column

Correspondence to:

S. A. Behnke, sbehnke@lanl.gov

Citation:

Behnke, S. A., Edens, H. E., Thomas, R. J., Smith, C. M., McNutt, S. R., Van Eaton, A. R., et al. (2018). Investigating the origin of continual radio frequency impulses during explosive volcanic eruptions. *Journal of Geophysical Research: Atmospheres*, 123, 4157–4174. https://doi.org/10.1002/2017JD027990

Received 31 OCT 2017 Accepted 9 MAR 2018 Accepted article online 13 MAR 2018 Published online 21 APR 2018

Investigating the Origin of Continual Radio Frequency Impulses During Explosive Volcanic Eruptions

S. A. Behnke¹, H. E. Edens², R. J. Thomas², C. M. Smith³, S. R. McNutt³, A. R. Van Eaton⁴, C. Cimarelli⁵, and V. Cigala⁵

¹Los Alamos National Laboratory, Los Alamos, NM, USA, ²Langmuir Laboratory, New Mexico Institute of Mining and Technology, Socorro, NM, USA, ³School of Geosciences, University of South Florida, Tampa, FL, USA, ⁴Cascades Volcano Observatory, U.S. Geological Survey, Vancouver, WA, USA, ⁵Department of Earth and Environmental Sciences, Ludwig-Maximilians-Universität München, Munich, Germany

Abstract Volcanic lightning studies have revealed that there is a relatively long-lasting source of very high frequency radiation associated with the onset of explosive volcanic eruptions that is distinct from radiation produced by lightning. This very high frequency signal is referred to as "continual radio frequency (CRF)" due to its long-lasting nature. The discharge mechanism producing this signal was previously hypothesized to be caused by numerous, small (10–100 m) leader-forming discharges near the vent of the volcano. To test this hypothesis, a multiparametric data set of electrical and volcanic activity occurring during explosive eruptions of Sakurajima Volcano in Japan was collected from May to June 2015. Our observations show that a single CRF impulse has a duration on the order of 160 ns (giving an upper limit on discharge length of 10 m) and is distinct from near-vent lightning discharges that were on the order of 30 m in length. CRF impulses did not produce discernible electric field changes and occurred in the absence of a net static electric field. Lightning mapping data and infrared video observations of the eruption column showed that CRF impulses originated from the gas thrust region of the column. These observations indicate that CRF impulses are not produced by small, leader-forming discharges but rather are more similar to a streamer discharge, likely on the order of a few meters in length.

Plain Language Summary This paper investigates the origin of a radio frequency (RF) signal previously termed "continual RF" that has been detected from the ash plumes of explosive volcanic eruptions. Continual RF had been hypothesized to be caused by many very small lightning-like discharges on the order of 100 m in length occurring at the vent of the volcano. To test this hypothesis, we conducted a multiparametric observational experiment at Sakurajima Volcano in Japan. We measured continual RF during eruptions of Sakurajima in 2015 and found that continual RF is a collection of short duration RF impulses, on the order of 160 ns in duration. These RF impulses are distinct from those typically produced by lightning. We also observed small, 30-m lightning discharges occurring near the volcanic vent that were distinct from the source of continual RF. Our observations show that continual RF is caused by an electrical discharge that is more simple than even a very small (~100 m) lightning discharge. We conclude that continual RF is caused by numerous, small, electrical discharges similar to streamer discharges, on the order of a few meters in length.

1. Introduction

Volcanic plumes are electrically charged and often produce lightning, which has been documented by many studies (Aizawa et al., 2016; Anderson et al., 1965; Arason et al., 2011; Behnke & McNutt, 2014; Behnke et al., 2012, 2013, 2014; Bennett et al., 2010; Brook et al., 1974; Cimarelli et al., 2016; Hoblitt, 1994; McNutt & Davis, 2000; McNutt & Williams, 2010; McNutt et al., 2010; Miura et al., 2002; Thomas et al., 2007, 2010; Van Eaton et al., 2016). One useful means of studying lightning is through measurements of very high frequency (VHF) radiation, of which lightning and other processes of electrical breakdown are copious producers. Previous studies of lightning in volcanic eruptions using VHF antennas have detected a source of VHF radiation that is distinct from lightning and is associated with the explosive ejection of ash (Behnke et al., 2012, 2013, 2014; Thomas et al., 2007, 2010). This radiation source is referred to as continual (or continuous) radio frequency (CRF) and manifests as relatively high rates of VHF radiation impulses

©2018. American Geophysical Union. All Rights Reserved.



(several thousands to over 10,000 impulses per second; Behnke et al., 2013) that occur over durations on the order of seconds or longer. By contrast, lightning is a discrete phenomenon, occurring on timescales on the order of tens to hundreds of milliseconds; thus, the VHF emissions from lightning are similarly short lived. The relatively long duration is one of the key characteristics that distinguish CRF radiation sources from those produced by lightning.

Observations of CRF have been made by Lightning Mapping Array (LMA) sensors (Rison et al., 1999; Thomas et al., 2004) during eruptions of Augustine Volcano (2006; Alaska, United States; Thomas et al., 2007, 2010), Redoubt Volcano (2009; Alaska, United States; Behnke et al., 2012, 2013), and Eyjafjallajökull (2010; Iceland; Behnke et al., 2014). Based on data collected during the Augustine eruption, it was hypothesized that CRF was caused by numerous, small (10–100 m), leader-forming discharges occurring at or near the vent of the volcano (termed "vent discharges"), which implied that the volcanic ejecta were charged upon eruption. The basis of this hypothesis was that the CRF radiation sources were relatively powerful, similar to the VHF emissions detected from discrete lightning discharges. Thus, it seemed most plausible that a similar process was producing the CRF, just on a smaller scale and at high rates over a long duration. The follow-on study at Redoubt confirmed that CRF occurred simultaneously with the onset of an explosive eruption and originated at low altitude, likely near the vent in the ash column. The data obtained at Eyjafjallajökull showed that there was a variation in the intensity of CRF among different eruptive events at the range of the VHF antennas. No further insight about the mechanism-producing CRF was gained from these subsequent studies.

It is significant that the overall, macroscopic form of the CRF signal (the collection of impulses at high rates over durations of seconds or tens of seconds) is conspicuous and distinct from VHF radiation produced by lightning (bursts of impulses lasting several hundreds of milliseconds). Since this CRF signal is not known to occur during meteorological thunderstorms, detection of CRF would be an unambiguous indicator of explosive volcanic activity. Thus, knowledge of the source mechanism would be useful for the application of VHF observations to volcano monitoring. Further, since the ash-charging mechanisms are processes inherent to magmatic fragmentation (e.g., fractoemission; Dickinson et al., 1988; James et al., 2000), turbulent ash flow, and eruption column dynamics (e.g., collisional charging; Cimarelli et al., 2014; Houghton et al., 2013; Mendez Harper & Dufek, 2016), study of the electrical activity may add to the understanding of explosive eruptions. CRF is also interesting from a lightning science perspective, as it provides insight into electrical discharge processes that produce VHF radiation.

This paper reports on the results of a multiparametric field campaign at Sakurajima Volcano in Japan that was designed in part to test the hypothesis that CRF is caused by small, leader-forming electrical discharges. In that regard, the main goals of the campaign were to see if (1) there was a detectable electric field change typical of leader stepping associated with CRF and (2) if there was any substantial visible light produced by CRF. The point of the second goal was to reconcile numerous visual observations and photographs of lightning near the vents of many volcanoes during explosive eruptions with VHF observations of electrical activity.

Figure 1 shows a map of the locations of the instruments that were installed around Sakurajima Volcano in May of 2015. Some of these instruments, like the LMA (indicated by circles), ran autonomously and collected data continuously over several months. Other instruments, such as high-speed video cameras, were manually triggered during an approximately 10-day period of 24-hr observations. These observations took place at the Sakurajima Volcano Observatory branch at Kurokami, which is located on the east side of Sakurajima Volcano and has an unobstructed view to Sakurajima's contemporaneously active Showa crater. In this section we describe the instrumentation that provided data for the analysis in this paper; however, we note that the experiment also involved seismic measurements, which will be reported on in separate papers.

A nine-station VHF LMA was deployed around the volcano such that each station had a line-of-sight view to Showa crater. Each lightning mapping station detects peaks in the logarithmically detected VHF waveform (66 to 72 MHz bandwidth), which is sampled at 25 MS/s. Global Positioning System (GPS) timing is used to time tag the peaks. The data from the sensors are then processed using time-of-arrival methods, which gives the locations of the VHF sources (the peaks in the waveform). The overall timing accuracy for the LMA system is about 30 ns (Thomas et al., 2004). In this study, the LMA was used both for locating sources of VHF radiation produced by electrical activity and for analysis of CRF by making use of the unprocessed data recorded by the individual stations. To maximize the location accuracy in the vertical dimension, LMA stations were deployed at locations of varying altitude (Figure 1); the altitude of the sites located on the mainland ranged between 60 and 630 m, while the sites on Sakurajima ranged in altitude between 40 and 105 m. Note that these

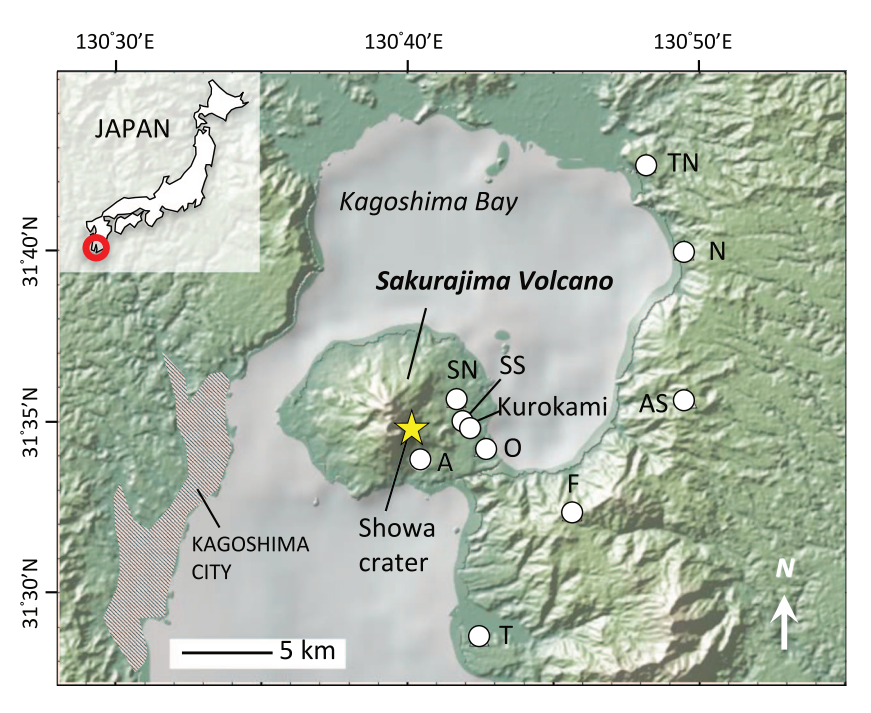


Figure 1. Map showing instrument sites for the Sakurajima volcanic lightning study. Lightning Mapping Array sensor sites are indicated by circles. The sites located on Sakurajima are Sabo North (SN), Sabo South (SS), Kurokami (K), Okuyama (O), and Arimura (A). The sites located on the mainland are Taniguchi (TN), Nakanochaya (N), Astronomy (AS), Forest (F), and Tarumizu (T). All nonautonomous sensors were located at Kurokami. Infrasound and seismic sensors were located at Kurokami and near the Sabo North site. The autonomous slow antenna was also located near the Sabo North Lightning Mapping Array site.

and all altitudes reported in this paper are GPS altitudes. The LMA was operating in 10-µs mode, meaning at most one peak is detected in each successive 10-µs time window.

A tenth lightning mapping station was located at the Kurokami observatory for the purpose of directly recording the log-RF waveform, which is normally peak detected by the LMA. This is achieved by splitting the output from the LMA's log amplifier and digitizing the log-detected waveform separately. In this configuration the LMA still also peak detects the waveform; therefore, this station also contributed to the determination of source locations. The waveform was digitized at 25 MS/s, and the manually triggered records were 6.7-s long (all pretrigger). Timing was acquired by digitization of the GPS pulse per second.

In addition to the log-RF antenna, a set of instruments that measure electric field changes, which are referred to as slow and fast antennas, were also located at the Kurokami observatory. Data collection was triggered manually. These data were digitized at 5 MS/s, and data records of 6.7 s (also all pretrigger) were recorded. The slow and fast antennas had time constants of 1 s and 0.1 ms, respectively. Continuous electric field change data were collected by an autonomous slow antenna, which was located near the Sabo North LMA station (SN in Figure 1). This instrument had a time constant of 15 s and a sample rate of 50 kS/s. A GPS receiver provided timing. The amplitudes of the slow and electric field change data represent the electric field but are presented in units of the instrument output voltage. The instrument is linear in response; thus, the electric field change is related to the output voltage by a calibration factor. We present the waveform amplitudes in arbitrary units.

Two high-speed video cameras were operated at the Kurokami observatory. The first was a Phantom v7.3 manufactured by Vision Research. This camera has a CMOS sensor of 800×600 pixels, GPS timing, and 16 GB of RAM. A frame rate of 6,400 frames per second (fps) and a lens of 105-mm focal length were used. The strategy for this camera was to collect the first few seconds following the onset of an explosive event in the hope of recording optical emission from CRF. The strategy for the second camera, a Phantom v711, also manufactured by Vision Research, was to trigger on lightning. This camera has a CMOS sensor of 1, 280 \times 800 pixels, 32-GB RAM, and GPS timing. Frame rates of 3,000 (for night use) and 5,000 (day use) fps were used. The camera was fitted with a lens of 100-mm focal length.

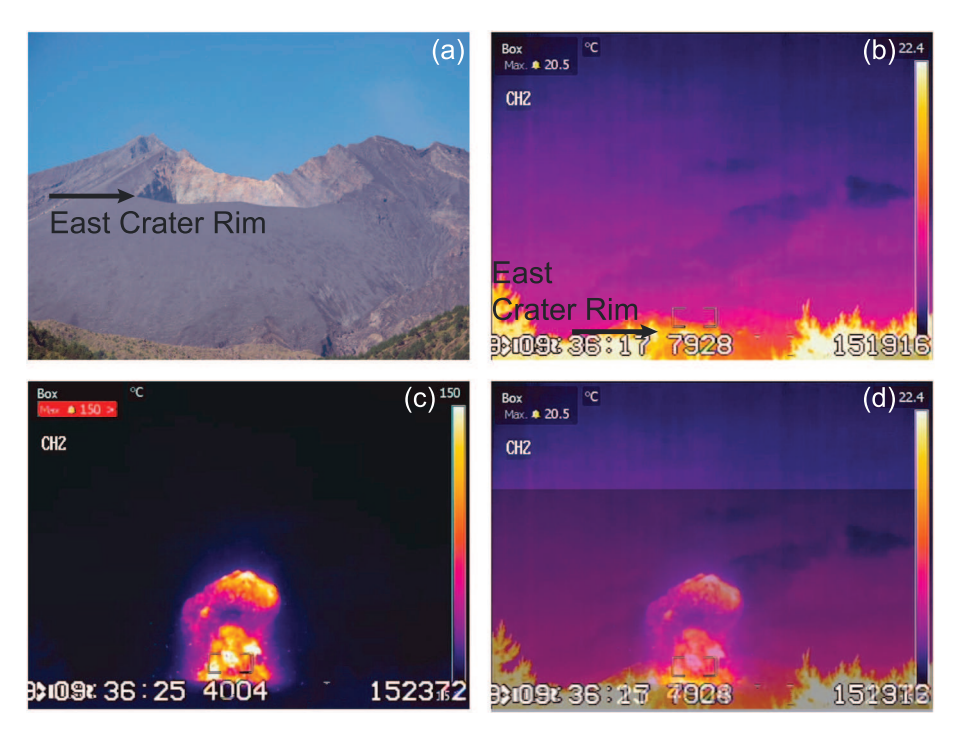


Figure 2. Comparison of visible light and infrared images. (a) Close-up view of Showa crater from Kurokami. The arrow indicates the eastern crater rim. (b) Infrared image of Showa crater, with arrow pointing to the eastern crater rim. Bright foreground features are trees that were located near the camera. (c) Infrared image taken during eruption. (d) Composite of images shown in (b) and (c). Color scales on (b)–(d) indicate temperature, and scaling is dynamic.

Observations of the eruption columns were made in visible and infrared wavelengths from the Kurokami observatory. A FLIR SC600 (640×480 pixels) was used for the infrared observations, and the data were recorded by two different means. Radiometric data were recorded on a PC using a manual trigger to start and stop recordings with a frame rate of 30 fps. In addition, a continuous stream of the FLIR images was recorded on a digital video recorder (DVR) via the camera's composite video output at 29.9 fps. A GPS video time inserter (model IOTA-VTI v3) was used to time tag the composite video output. The DVR used was a Lorex ECO4, which had a recording resolution of 960 × 480 pixels and a 1-TB hard disk drive. The time-tagged data were used to obtain time series of the eruption column height using photogrammetric methods with MATLAB software developed by Valade et al. (2014). The timing for the radiometric data was acquired by manually matching frames between the GPS time-tagged composite video data and the radiometric data. Figure 2 shows the field of view of the infrared camera and provides context for the infrared images shown in section 2 by comparing a visible light photograph to infrared images before and during eruption.

In the visible spectrum, video observations were made with a high-sensitivity camera (Watec 910 HX/RC, NTSC model). This camera has a resolution of 768×494 pixels and minimum sensitivity of 0.0000025 lux (0.0001 lux corresponds to the light level of the background sky on a moonless night). An auto-iris lens with adjustable 4- to 8-mm focal length was used. The images from this camera were also time tagged with a video time inserter and recorded continuously on the same DVR as described above. The camera ran continuously throughout the field campaign and helped to identify when explosive events occurred.

Infrasound data were collected from two sites: the Kurokami observatory and near the Sabo North LMA station. InfraBSU sensors (manufactured at Boise State University) were used at both sites. The sensors had a range of ± 125 Pa and a low cutoff frequency of 0.048 Hz. Three sensors were used per array; one array was located at each site. Data were digitized by a Nanometrics Centaur digitizer, which has a 24-bit Analog-to-Digital Converter. Sample rates of 100 S/s were used. Seismic sensors were also hosted at both the Kurokami and Sabo North sites.

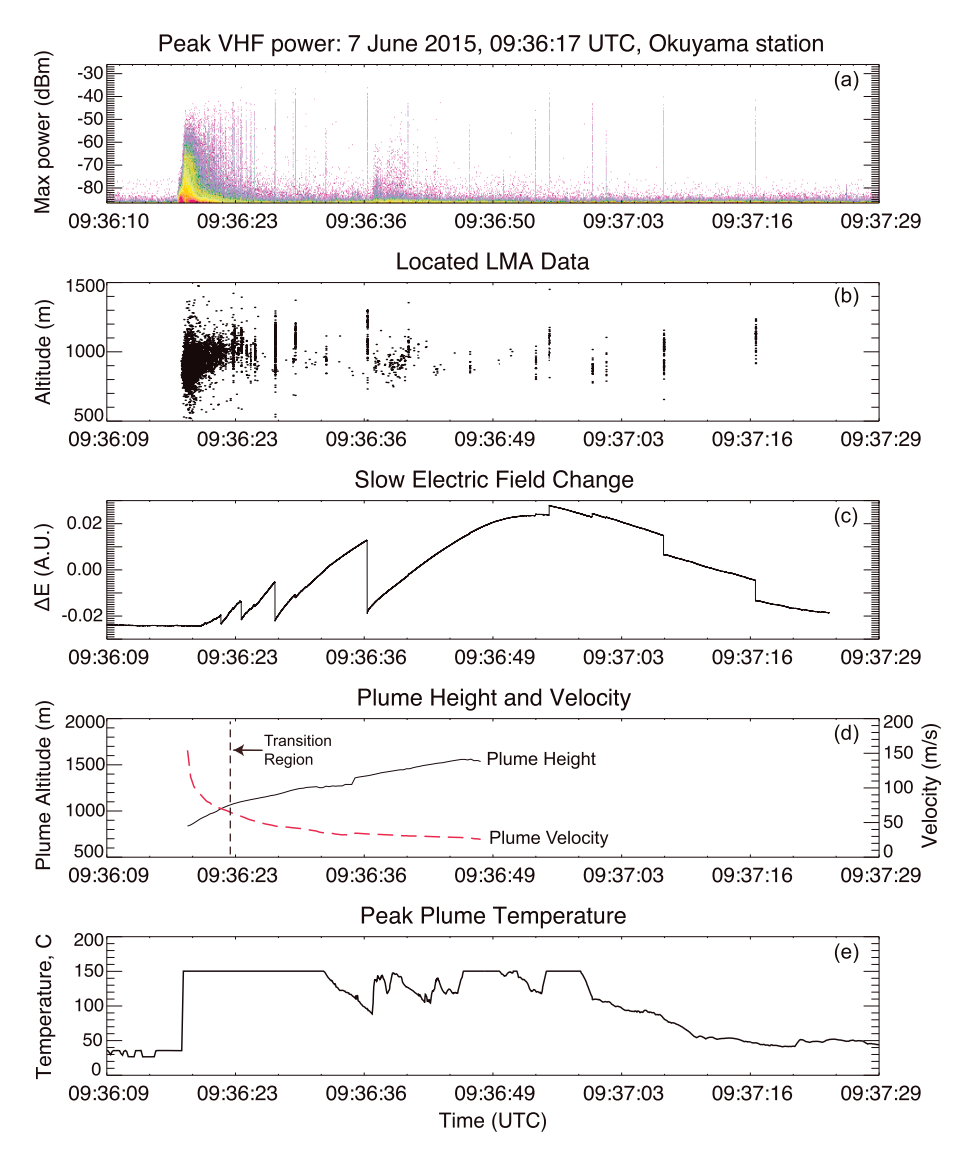


Figure 3. Comparison of LMA, electric field change, and eruption column observations for the explosive event on 7 June 2015 at 09:36:17 UTC. (a) Unprocessed Lightning Mapping Array (LMA) data from the Okuyama station showing received power versus time, plotted as a two-dimensional event density histogram. Color indicates relative density of events, with red indicating the highest event density and purple the lowest event density. (b) Located LMA data, plotted as (Global Positioning System) altitude versus time of individual very high frequency (VHF) sources. (c) Slow electric field change data from the Sabo North slow antenna, presented in arbitrary units. (d) Eruption column height (altitude referenced to Global Positioning System, black solid line) and velocity (red dashed line) versus time as determined through photogrammetric analysis of the time-stamped infrared images. The dashed vertical line indicates the transition region from momentum-driven ascent to buoyancy-driven ascent. (e) Peak eruption column temperature versus time as determined from the radiometric infrared data. Note that data clipping occurred when the temperature exceeded the threshold settings of the camera. UTC = universal time coordinated.

2. Observations

During the May–June field campaign, hundreds of short, discrete explosions classified as Vulcanian eruptions occurred at the Showa crater (770 m) of Sakurajima, and CRF was detected during many of these events. Plume heights typically reached 2 or 3 km in altitude, corresponding to 1.2–2.2 km above the vent. CRF was observed in association with the explosive activity, and the rate and strength of CRF declined over time following an explosion. Figure 3a shows CRF occurring contemporaneously with onset of the 7 June 09:36:17 explosive event (hereafter referred to as event 0607-093617), as inferred by the step change in the peak eruption column temperature (Figure 3e). The CRF rate decreased over roughly 2 s (inferred from event density

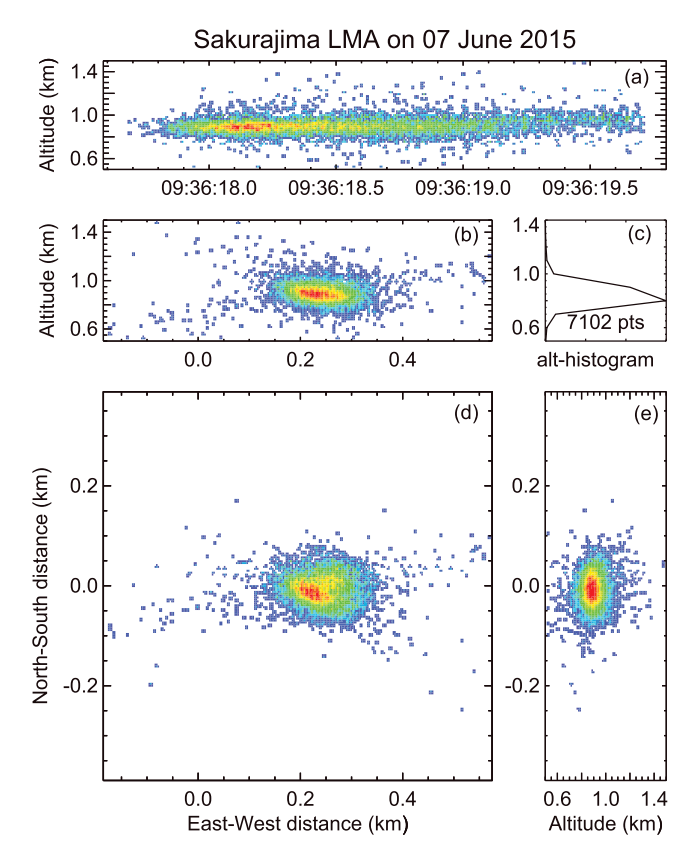


Figure 4. Locations of continual radio frequency sources as detected by the Lightning Mapping Array (LMA) during the first 2 s following the onset of the explosive event at approximately 09:36:17 on 7 June 2015, plotted as relative event density, where blue represents the lowest density of events and red represents the highest density of events. Altitudes are referenced to Global Positioning System. (a) Time series of the altitude of the located very high frequency sources. (b) Altitude versus east-west position. (c) Altitude histogram of the sources. (d) Plan view plot of the located sources. (e) Altitude versus north-south position.

histograms in Figures 3a, 4a, and 6a), and discrete lightning discharges began to occur (vertical lines in event density histograms, Figures 3a and 6a). An increase in CRF rate occurred at approximately 09:36:36.4, coincident with an increase in peak eruption column temperature (Figure 3e) indicating renewed vigor in the ongoing explosive event. The observation of CRF occurring at the onsets of explosive events is consistent with previous observations from Augustine and Redoubt Volcanoes, though CRF occurred over durations on the order of tens of seconds during those explosive eruptions (Behnke et al., 2013; Thomas et al., 2007, 2010). The Augustine and Redoubt eruptions were larger and more energetic (plume heights between 10 and 20 km), which likely accounts for this difference. The onset of CRF at Sakurajima prior to the onset of detectable, discrete lightning is also consistent with previous observations.

The LMA data show that CRF was confined to relatively low altitudes within the eruption column in comparison to the vertical extent of lightning. In the example shown in Figures 3 and 4 for event 0607-093617, CRF sources were generally located below 1 km (230 m above Showa crater), while lightning discharges had extents more than twice as high, up to 1.3 km (530 m above Showa). This difference corresponds to an important transition in the dynamics of the eruption column. Previous studies have shown that the transition from momentum-driven (gas thrust) ascent to buoyancy-driven (convective) ascent is marked by a significant decrease in the deceleration of the eruption column (Dürig et al., 2015). This is sometimes referred to as a "kink" in the velocity profile. The transition occurs when the density of the eruption column has decreased enough to be equal to that of the surrounding atmosphere (e.g., Figure 1 of Mastin, 2007). In Figure 3d we infer this transition to have occurred at approximately 1.1 km (330 m above Showa crater), where there is also an obvious change in the slope of eruption column height time series. This indicates that CRF sources were likely confined to the dense, gas thrust region of the eruption column, while lightning extended up into the buoyant region of the eruption column.

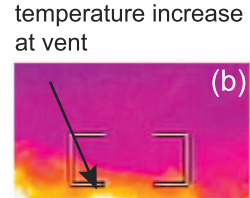
Comparison between the single-station unprocessed LMA data and the infrared data for event 0607-093617 revealed that CRF sources were being

detected before the eruption column came into view of the camera at the Kurokami observatory. Figure 5 shows four frames from the infrared camera, showing that the eruption column appears at approximately 09:36:17.8262. Figure 6 shows that the Okuyama LMA station started detecting CRF at approximately 09:36:17.35, about 500 ms before the eruption column was visible on the infrared camera. Given the geometry between the crater and the Okuyama and Kurokami sites (see Table 1), the additional altitude that the eruption column would need to gain in order to come into the line of sight at Kurokami compared to Okuyama would be on the order of only 5 m $\pm \sim 22\%$. An eruption column with vertical velocity of 150 m/s (estimated from Figure 3) would gain an altitude of 5 m in about 33 ms, which is much less than the observed delay of 500 ms. This implies that the LMA was detecting radiation originating below the rim of the crater that was most likely being scattered (i.e., the radiation was reflected or diffracted; we use the term "scattering" as a general term) by the crater walls. Figure 6a also shows that the detected power of the CRF sources increased after the eruption column came into the line of sight of the Okuyama antenna, which would be expected as there would likely be some initial attenuation in the CRF source power due to scattering.

Comparison of VHF source arrival time differences between two sensors provides further evidence that the LMA detected VHF sources indirectly before the eruption column came into the line of sight of the sensors. Figure 7a shows arrival time differences between the Okuyama and Sabo South LMA stations during an event on 4 June at 01:48:07. Generally speaking, the arrival time difference of a VHF source between two sensors corresponds to source locations that are anywhere along a hyperbola that lies between the sensors. Prior to the eruption column coming into the line of sight, an LMA sensor could detect radiation that is scattered off the crater walls, for example, which would produce the large spread in arrival time differences in Figure 7a







First indication of



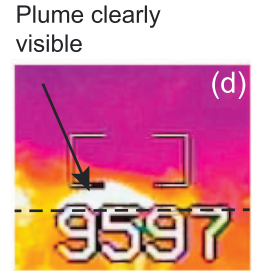


Figure 5. The onset of the eruption from the view of the infrared camera. The increase in temperature at the crater rim indicates an eruption column beginning to enter the line of sight. (a) 09:36:17.7928: just prior to eruption; full frame. (b) 09:36:17.8262: slight increase in temperature detected at the crater rim; cropped frame. (c) 09:36:17.8929: increase in temperature at crater rim is more pronounced; cropped frame. (d) 09:36:17.9597: clear indication of the eruption column above the crater rim; cropped frame.

(shown as a yellow band centered around 7 s on the x axis). These sources are also relatively weak, as shown in Figure 7b. After the eruption column came into view, the spread in arrival time difference decreased, and more distinct bands of arrival time difference are visible (indicated by arrows). In Figure 7a arrival time differences corresponding to the azimuth angle of Showa crater are indicated, along with other correlations corresponding to the azimuths away from Showa. Those correlations at azimuths away from Showa would be expected due to propagation delays arising from indirect signal paths. Figure 8 shows a map of the arrival time difference hyperbolas and a histogram of arrival time differences for 50 ms of data when CRF was occurring. The histogram shows a dominant peak at a time difference of about 3.8×10^{-6} s and a smaller peak at about 4.7×10^{-6} s. The main peak corresponds to the azimuth of Showa crater, and the corresponding hyperbolas are shown passing over Showa on the map in Figure 8. The lesser peak corresponds to a hyperbola falling to the north of Showa (also plotted in the map), and we conclude that these source's arrival times were delayed at the LMA sensors, which could occur due to scattering.

The LMA data also show that the power of the CRF sources was similar to that of the weakest sources produced by discrete lightning. The source power of the located CRF sources occurring between 09:36:17.75 and 09:36:19.0 during event 0607-093617 ranged between -28 and 5 dBW, as shown in Figure 9. This range of source powers is comparable to the range of source powers of CRF for the other events observed from Sakurajima but does not extend as high as those produced by discrete lightning from the Sakurajima events. For example, source powers for the time period dominated by discrete lightning (09:36:21-09:36:38) ranged from -27 to 18 dBW. Additionally, the peak in the source power distribution for CRF increased by a factor of 2 (-18.9 to -15.1 dBW) after the eruption column came into the line of sight of the sensors, which would be expected if at least some of the sources of CRF also came into direct view of the sensors.

The electric field change data (Figures 3 and 6) indicate that the eruption column did not initially carry a net charge that was detectable by the autonomous slow antenna—suggesting that the charge in the column was initially well mixed—and that CRF was occurring in the absence of a large-scale, net static electric field. During event 0607-093617 the first detectable change in the electric field occurred at approximately 09:36:18.6, about 1.25 s after the first CRF radiation sources were detected by the Okuyama LMA. The field increased in the positive direction for approximately 175 ms before the field was reduced by a small lightning discharge occurring between the eruption column and the ground at approximately 09:36:18.816. Following this lightning discharge, the field recovered and then a series of small, step-like reductions in the field occurred starting at 09:36:19.07, likely due to the small lightning discharges. Some of these discharges can be seen in Figure 6a as vertical lines in the event density histogram. At 09:36:19.65 the electric field began to increase dramatically, indicating that the eruption column developed a net charge, likely due to differential settling speeds of oppositely charged ash particles. At the time when the electric field began to increase, the rate of CRF was declining.

The near-vent lightning discharge that occurred at 09:36:18.816 during event 0607-093617, which produced the field change shown in Figure 6, was also captured on high-speed video. As shown in Figure 10c, the discharge had a vertical extent of at least 30 m and occurred when the top of the eruption column was 70 m above the rim of the crater. The discharge is clearly distinguishable from the CRF activity in the raw and pro-

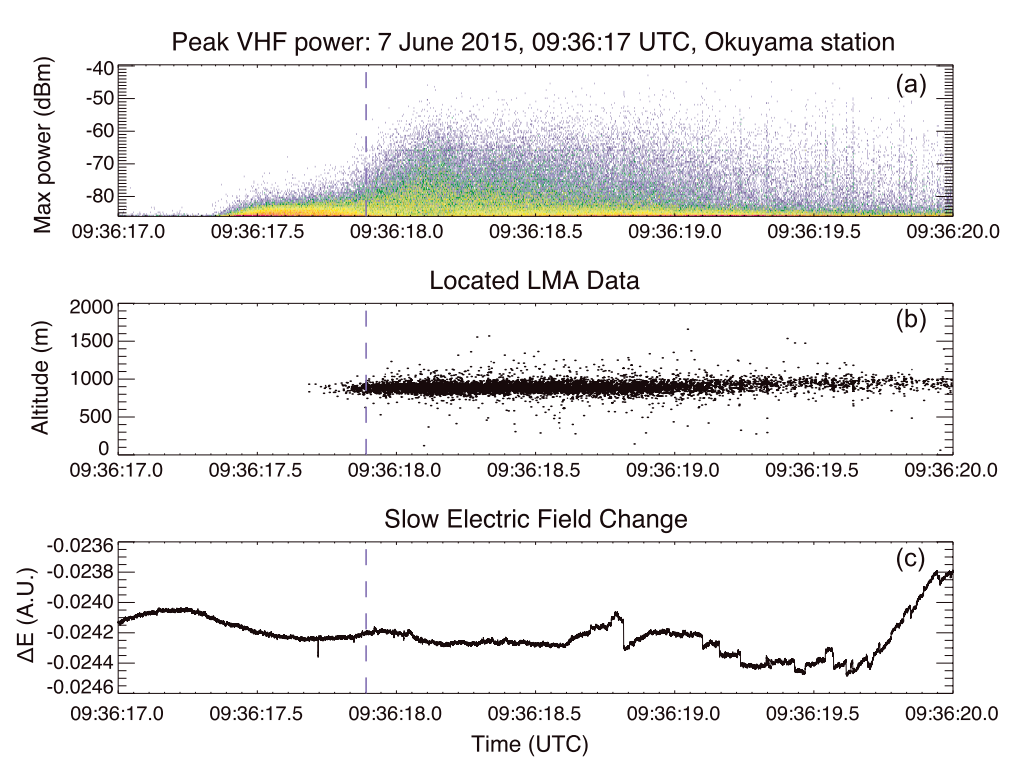


Figure 6. Lightning Mapping Array (LMA) (unprocessed and located) and electric field change data during the first few seconds following the onset of eruption. The dotted line at 09:36:17.8262 shows the time when the eruption column first came into the line of sight at Kurokami. (a) Unprocessed LMA data from the Okuyama stations, showing that radiation from CRF was first detected approximately 0.5 s prior to the eruption column coming into view at Kurokami. Note the increase in source power following the line-of-sight transition. (b) Few very high frequency (VHF) sources were located before 09:36:17.8262 due to the vent geometry. (c) No significant electric field changes were associated with the initial period of continual radio frequency. UTC = Universal Time Coordinated.

cessed LMA data. At the time of the discharge, the unprocessed LMA data show an increase in power relative to the background of CRF sources (rectangle in Figure 10a) while the processed LMA data show a cluster of sources occurring to the south of the located CRF sources (oval in Figure 10b), which is consistent with the location of the discharge in the high-speed video. These observations provide a bound on the scale of the electrical discharge that produces CRF: lightning discharges on the order of tens of meters are not the source of CRF.

The fast electric field change data show that the mechanism-producing CRF did not result in a significant transfer of charge. The fast antenna sensor deployed at Sakurajima detects changes in the electric field occurring between 0.5 and 100 μ s, and the magnitude of the field change arises from a combination of the amount of charge transferred and the distance over which it is transferred. Typical lightning leader steps occurring

Table 1 Geographical Data Used to Determine Line-of-Sight Difference Between Okuyama and Kurokami LMA Stations			
Feature	Value	Uncertainty (%)	Method
Okuyama altitude	43 m	~ 1	GPS
Kurokami altitude	63 m	~ 1	GPS
Distance between Okuyama and Showa	4,610 m	< 10	GPS
Distance between Kurokami and Showa	3,712 m	< 10	GPS
Altitude of Showa's east crater rim	770 m	< 1	Laser rangefinder
Width of Showa crater (east to west)	300 m	<1	Laser rangefinder

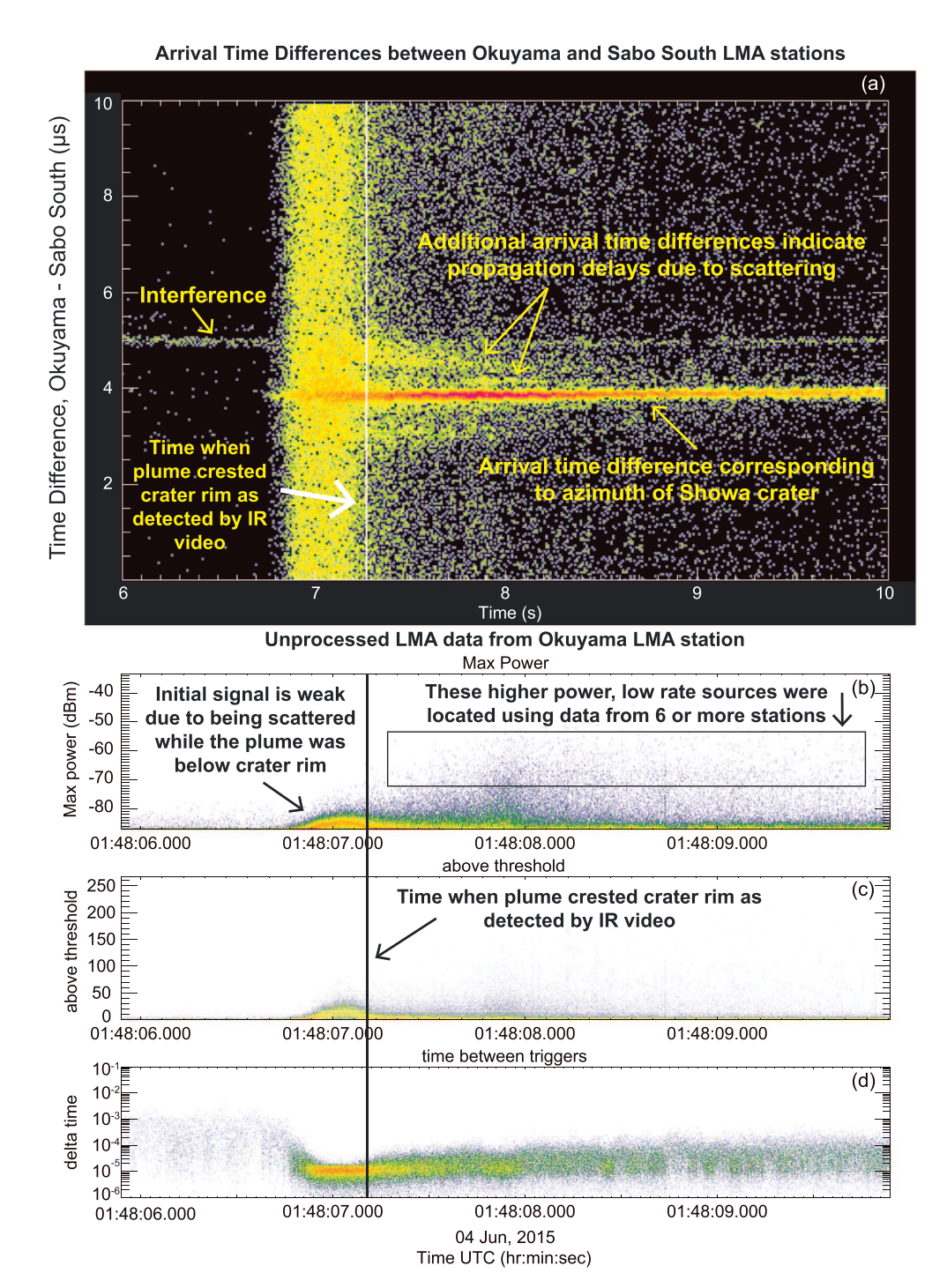
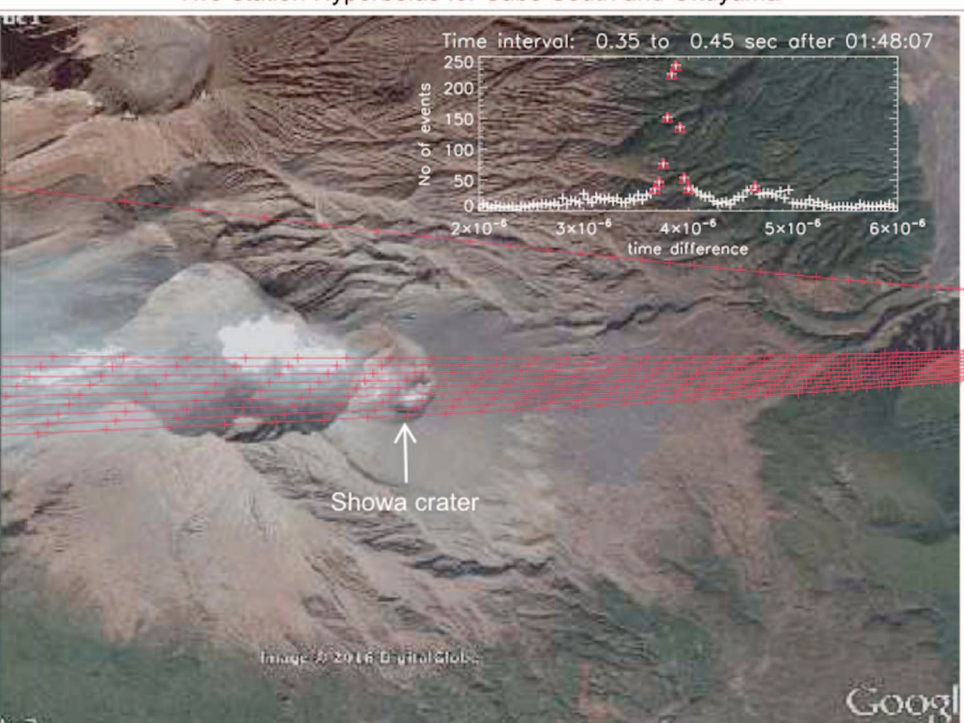


Figure 7. Unprocessed Lightning Mapping Array (LMA) data for the explosive event at 01:48 on June 4 2015. (a) Arrival time differences between sources detected by the Okuyama and Sabo South stations, plotted as delta-t versus time. (b) Peak power of radiation sources detected by the Okuyama station versus time. (c) Number of samples within each 10 μs window where the received power was above the background power threshold, shown as an event density histogram. The LMA only records one power value per window; therefore, the above threshold gives a sense of how many other events may have also occurred in that time window. (d) Time between subsequent events recorded by the LMA, shown as an event density histogram.



Two-station Hyperbolas for Sabo South and Okuyama

Figure 8. Map showing arrival time difference hyperbolas (pink plus marks connected by pink lines) for very high frequency sources detected by the Okuyama and Sabo South stations during a period of the 01:48 on 4 June event when continual radio frequency was detected. The histogram shows arrival time difference correlations. Red on the main peak corresponds to the hyperbolas drawn on the map that pass over Showa. A secondary peak occurs around a time difference of $4.7~\mu s$, which corresponds to an azimuth that lies north of Showa.

during thunderstorm lightning manifest as impulses lasting several microseconds due to fast charge transfer. During the Sakurajima campaign, no fast electric field changes were detected in conjunction with CRF. Figure 11 shows an example of a CRF impulse from the log-RF antenna and the associated fast antenna data; the CRF impulse is on the order of 160 ns in duration, and there was no field change associated with the impulse. The 160-ns duration is comparable to the impulse response of the 6-MHz band-pass filter that the LMA uses. Therefore, 160 ns is the upper limit of the duration of the CRF impulses.

Fast electric field changes were detected during the campaign from discrete lightning discharges; however, it is not clear if any electric field changes due to leader stepping were detected. Figure 12 shows log-RF (a), fast electric field change (b), and slow electric field change (c) for a short duration (6 ms) lightning discharge. The step changes shown in Figure 12c were likely caused by charge transfer during a return stroke. The first fast pulse shown in Figure 12b is reminiscent of an initial breakdown pulse. The other low-amplitude fast pulses in Figure 12b may be due to K-events (also known as recoil events or recoil leaders; Shao & Krehbiel, 1996; Winn et al., 2011). We could not identify pulses that are unambiguously associated with leader stepping in the fast antenna waveform data.

There were also no obvious optical emissions detected by high-speed video that were correlated with CRF. Many small lightning discharges were detected by high-speed video during periods with CRF, but these were all correlated with lightning discharges detected by the LMA (e.g., Figure 10). This observation could mean that the mechanism producing CRF is either not optically bright or is occurring within the optically dense eruption column.

As described at the beginning of this section, CRF was typically observed concurrent with an explosive eruption, and larger lightning typically occurred after CRF rates declined and once the eruption column had developed beyond the gas thrust phase. However, there were some cases where larger lightning occurred

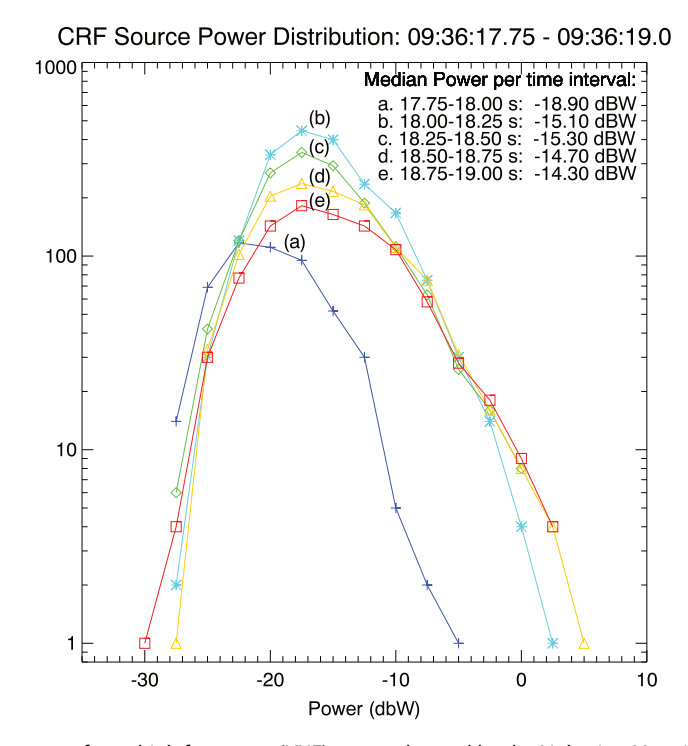


Figure 9. Power histograms of very high frequency (VHF) sources located by the Lightning Mapping Array for the first 1.25 s following the onset of the explosive event on 7 June 2015 at 09:36:17. Each histogram corresponds to 0.25 s of data. CFR = continual radio frequency.

while CRF was also occurring, and in these cases the discharges temporarily affected the rate of CRF. For example, on 29 May there was an explosive event at approximately 00:05:17 that produced a brief burst of CRF and lightning (Figures 13a and 13b). About 16 s later, at 00:05:32, a second event occurred that produced a longer-lasting burst of CRF and lightning. The subsequent event occurred after a net electric field had developed as a result of charge separation in the eruption column produced by the first explosive event (Figure 13c). Several large lightning discharges occurred about 4 s after the onset of the second event while CRF was also occurring. The discharge shown in Figure 14 produced a significant change in the electric field (Figure 14d), and immediately following the discharge the rate and power of the CRF was temporarily reduced (Figures 14a and 14b), suggesting that the field change produced by the discharge affected the production of CRF. Several of the subsequent discharges occurring within the next few seconds also showed a similar effect on the CRF. This observation was not typical: during this campaign CRF usually occurred in the absence of a net electric field and the larger lightning discharges usually did not occur while CRF was occurring. Larger lightning usually occurred after the eruption column was more developed and after CRF (and the explosion) had waned. However, this particular eruptive sequence (two CRF-producing events occurring within a short time period) was also not typical during this monitoring campaign.

3. Discussion

The observations show that the physical process producing CRF impulses has the following characteristics: (1) It can occur in the absence of a large-scale electric field (Figure 6c); (2) it is not associated with a process that results in significant transfer of charge (Figure 11d); (3) the VHF radiation produced by CRF is relatively powerful (Figure 9); (4) the upper limit on the duration of a CRF impulse is approximately 160 ns (Figure 11c); (5) it occurs near to the vent and in our observations appears to be confined to the gas thrust region of the eruption column (Figures 3b, 3d, 4), and 6). It may not be an optically bright process. In addition, we observed that relatively large-scale lightning can temporarily reduce the production of CRF, presumably due to the electrostatic field change associated with the lightning, though this was only observed in rare cases where a second, CRF-producing eruptive event occurred in close succession to a previous event.

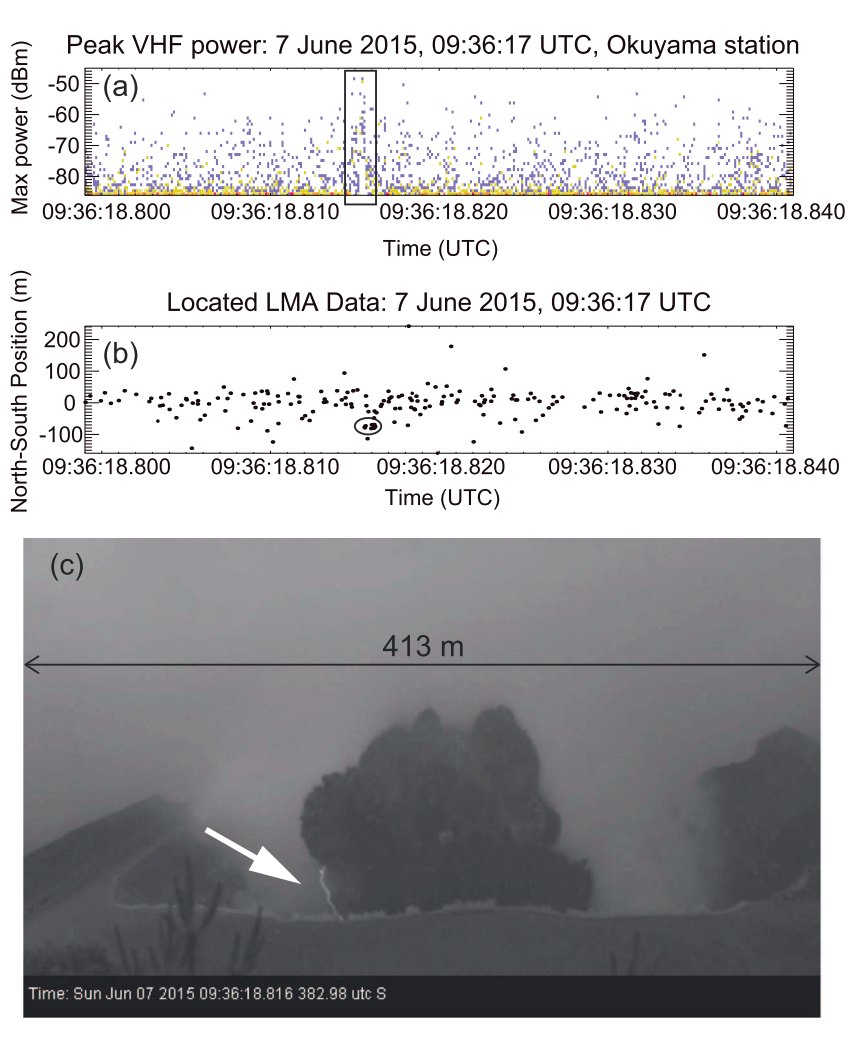


Figure 10. Example of a small lightning discharge captured on high-speed video and the corresponding Lightning Mapping Array (LMA) data. (a) 40 ms of unprocessed LMA data during the time when the discharge shown in (c) was detected (indicated by black rectangle). (b) The located LMA data corresponding to the time period shown in (a). The discharge shown in (c) is indicated by the black oval. (c) High-speed video frame showing a small lightning discharge on the left side of the eruption column extending from the eruption column to the crater rim. VHF = very high frequency; UTC = Universal Time Coordinated.

Overall, the observations do not support the original hypothesis that CRF is produced by numerous, small, leader-forming (hot) discharges. CRF and lightning discharges on the order of tens of meters in length were observed to be distinct processes (Figure 10). Furthermore, the duration of individual CRF impulses in the log-RF waveform is no greater than 160 ns (Figure 11c), which is an order of magnitude shorter than that of typical leader steps, which are on the order of several microseconds (Hill et al., 2011). Additionally, the fast antenna did not detect charge transfer associated with individual CRF impulses (Figure 11d); however, leader steps were also not detected because they were likely either too small or did not transfer enough charge to be detected. Fast antenna data did show charge transfer associated with initial breakdown pulses, return strokes, and K-events in small lightning discharges (Figure 12). Finally, no obvious optical emissions were detected in association with CRF; however, eruption columns are extremely optically dense; thus, we would not expect to see optical emissions from the interior of the plume, and the chances of detecting optical emissions from discharges on the column boundaries may be very low as well.

The observation that CRF sources have a short duration (~160 ns) suggests that CRF is associated with a process that is simpler than the formation of a leader. A leader can be described in simple terms as a self-sustaining, hot (5000–10000 K; Bazelyan & Raizer, 2000), plasma channel that grows and sustains its conductivity due to streamers at or near the tip of the leader. Thus, the formation of a leader is a compound

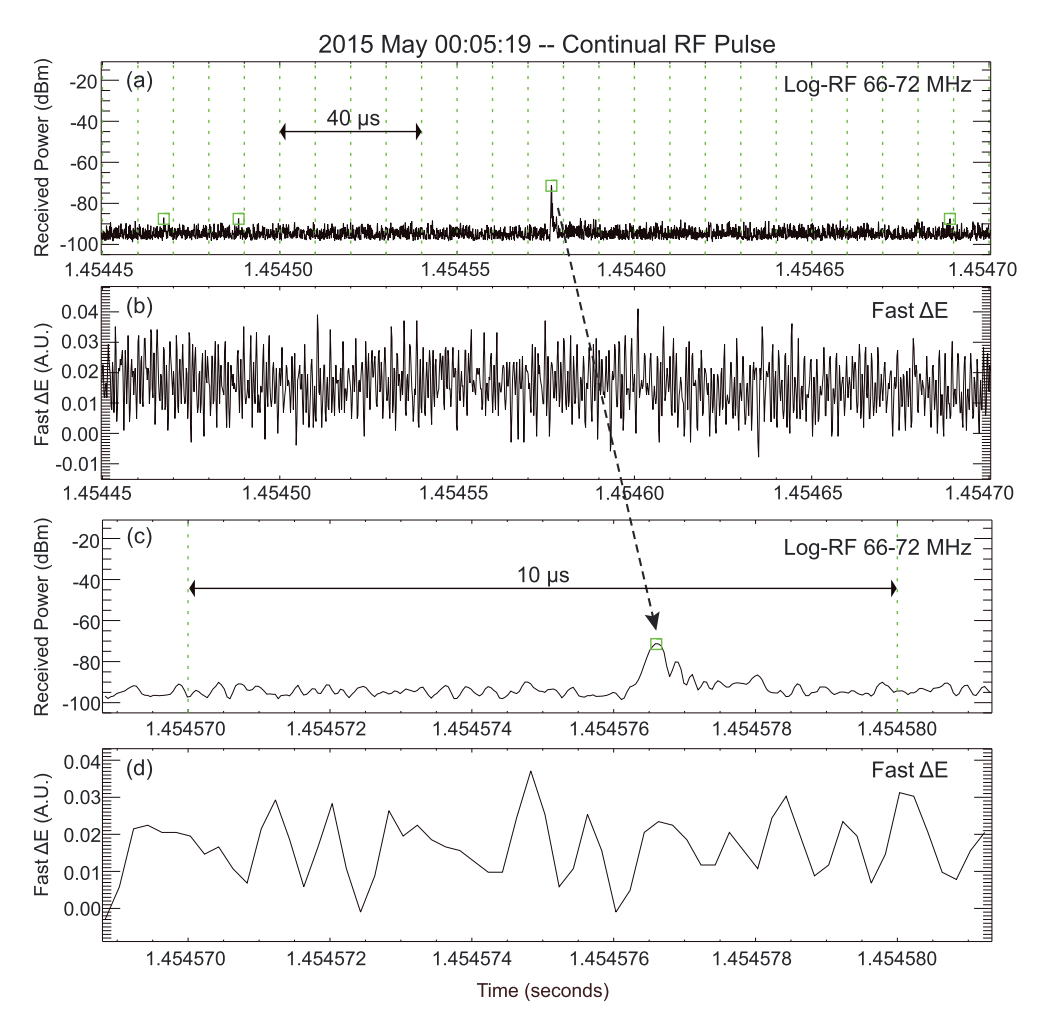


Figure 11. Log radio frequency (log-RF) and fast electric field change waveforms of a single continual radio frequency (CRF) impulse occurring during the explosive event on 29 May 2015 at 00:05 UTC. (a) 250 μs of log-RF very high frequency (VHF) data. Green squares indicate peak detections by the Kurokami Lightning Mapping Array (LMA) station, which provided the log-RF waveform. The CRF event has a peak power of about –70 dBm. The other three peak-detected events are likely noise. (b) Fast electric field change data during the period of the CRF impulse, indicating no significant transfer of charge during this time period. Waveform amplitudes presented in arbitrary units (A.U.). (c) Same as (a) but on an expanded scale showing the CRF impulse in more detail. (d) Same as (b) but on an expanded scale. Vertical green dotted lines in panels (a) and (c) indicate the 10 μs window boundaries of the LMA station.

process. If CRF is not caused by leader formation, the next logical process to consider as a candidate is some type of "cold" plasma discharge, that is, a plasma channel that is not sufficiently heated to maintain conductivity, such as a streamer or an electron avalanche. These are related processes, as streamers are created by repeated electron avalanches at the tip of the streamer (Gallimberti et al., 2002). We expect that a single electron avalanche would not itself be powerful enough to be detectable in the passband of the LMA (Cooray & Cooray, 2012) and thus hypothesize that a streamer discharge of some variety may be the source of CRF.

In the volcanic context there are several ways that streamers could be occurring near the vent, including corona breakdown on the crater or on ash particles, small streamer discharges between particles, or streamer discharges between pockets of charge in the eruption column. It is an open question as to which of these processes the LMA could have detected during the Sakurajima observations. The LMA has detected and located corona on towers and windmills during thunderstorms (Wu et al., 2017) and on airplanes passing through charged clouds (Hamlin, 2004). The source powers of CRF are in the range of the source powers of corona on towers and windmills (Wu et al., 2017). However, we do not know quantitatively the thresholds on the strength of corona or streamer discharges required for detection by the LMA. The radiation produced

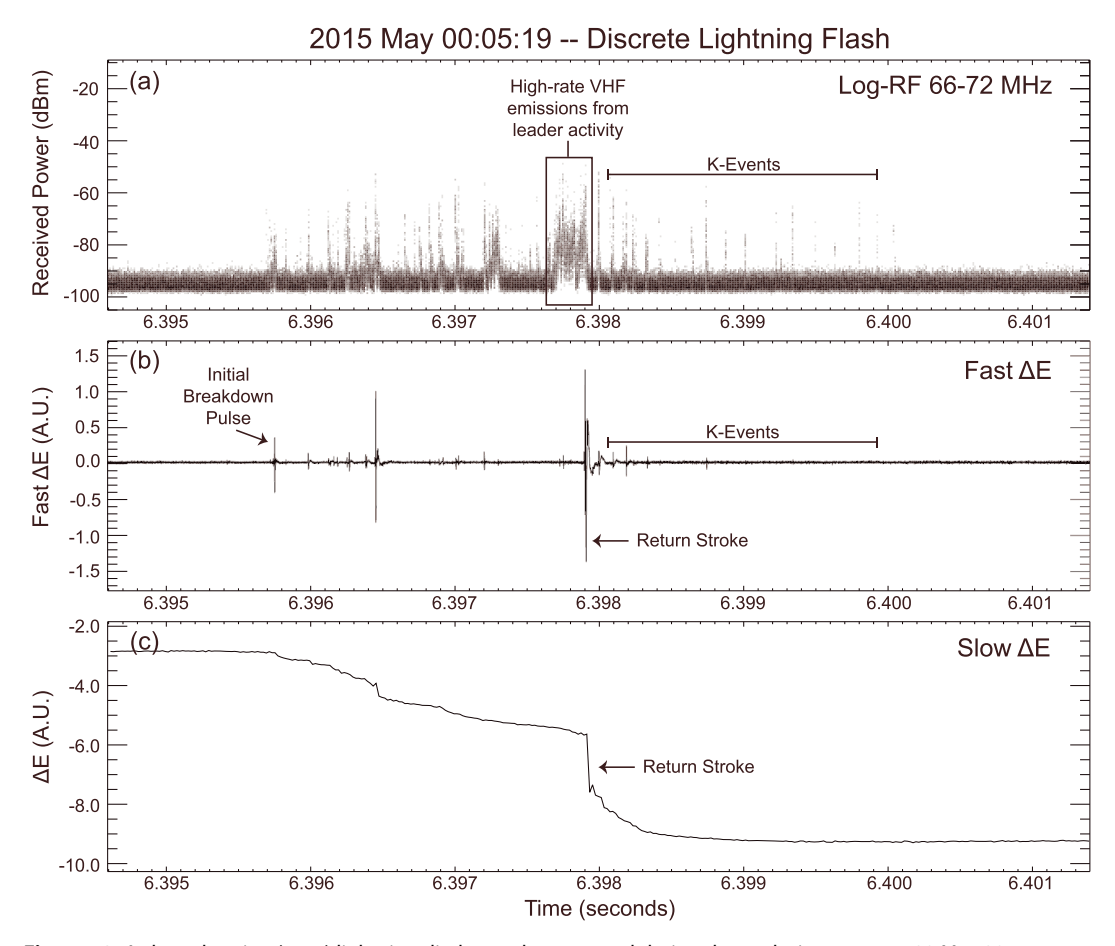


Figure 12. A short duration (5 ms) lightning discharge that occurred during the explosive event on 29 May 2015 at 00:05 UTC. (a) Log radio frequency (log-RF) data of the discharge, plotted as an event density histogram, where darker shades of gray indicate a higher density of events. Prominent features include very high frequency (VHF) emissions from leader activity (box) and impulsive VHF emissions from K-Events. (b) Fast electric field change data, showing an initial breakdown pulse, a return stroke, and several K-Events. (c) Slow electric field change data. The stepwise decrease in the electric field indicates that a return stroke occurred.

by so-called precursor discharges and narrow bipolar events, both of which are caused by fast positive breakdown (Rison et al., 2016), is also detectable by the LMA. However, the fast positive breakdown studied by Rison et al. (2016) occurred at higher altitudes (8 km and higher) and the length scales of those phenomena were several hundred meters. The characteristics of fast positive breakdown occurring near sea level (or in the gaseous environment of an eruption column, for that matter) are unknown and may be different. It is therefore not clear that the CRF process, which occurs on length scales of the order of meters, would be related to it.

Of all these processes, corona breakdown on the rim of the crater is least likely to be contributing to the CRF signal. This is because the slow antenna measurements showed that CRF usually occurred in the absence of a net electrostatic field, indicating that the charge in the eruption column was initially well mixed. Generally, by the time a net charge was detected in the eruption column, source rates of CRF had significantly waned (Figure 3), whereas one would expect corona rates to increase after a detectable net charge developed. Thus, corona on the crater rim is not likely to be the primary source of CRF.

CRF may have been caused by small streamer discharges between small pockets of charge or individual charged particles. Our observations show that CRF was originating from the gas thrust region (Figures 3b, 3d, and 4), which would have higher particle density and increased turbulence compared to the buoyant region of the eruption column. Cimarelli et al. (2014) showed that small electrical discharges can be produced in the turbulent flow of volcanic ash created by shock tube experiments. They proposed that turbulent flow promoted ash collisions and helped separate particles with differing Stokes numbers resulting in charge separation and small electrical discharges, on the order of a few centimeters in length. In these experiments,

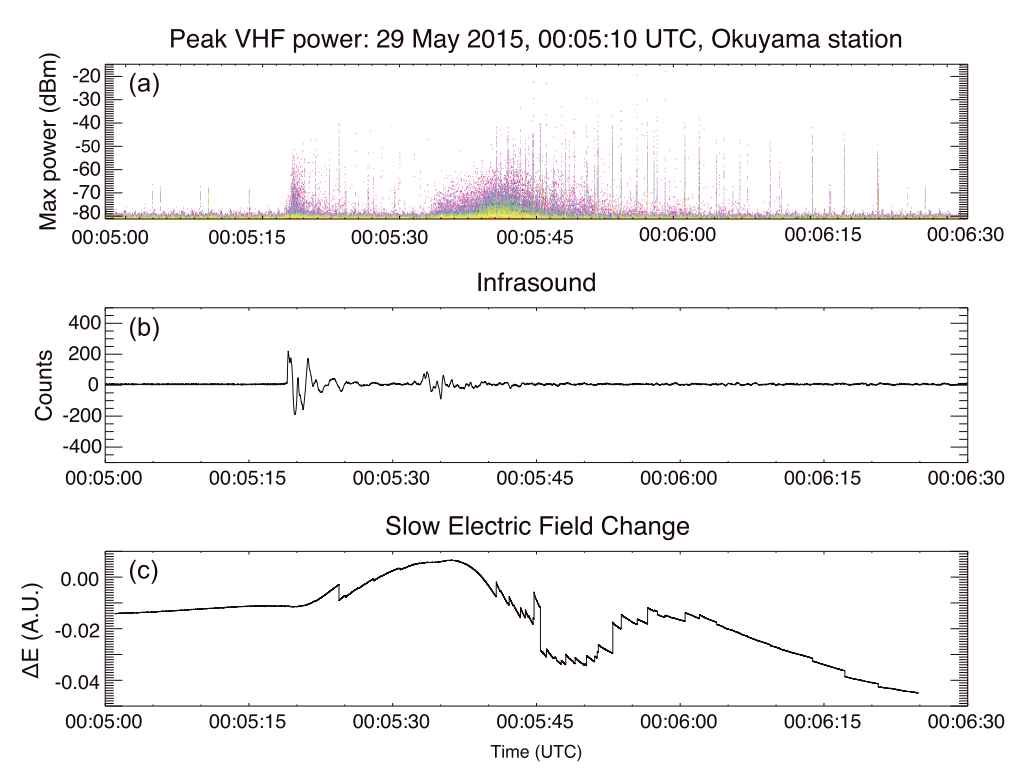


Figure 13. Continual radio frequency (CRF) and lightning that occurred during two explosive events on 29 May at approximately 00:05:17 and 00:05:32. (a) Unprocessed Lightning Mapping Array data, plotted as an event density histogram. (b) Infrasound data from the 'A' sensor at the Kurokami observatory. Data have been time shifted to account for the propagation time of the signal. (c) Electric field change data during the period of the two explosive events. The second explosive event occurred after a net static field had developed. VHF = very high frequency; UTC = Universal Time Coordinated.

the pressure at the nozzle was initially high when the ash particles were first expelled out of the shock tube, and over a period of few milliseconds the pressure at the nozzle decreased. The discharges were detected nearly simultaneous with the expulsion of ash and decreased in rate as the pressure decreased. This is similar to our observed behavior of CRF: it correlated in time with the onset of explosions, and the rate of CRF impulses decreased over time as the explosion waned.

CRF could also be caused by corona-like discharges occurring on charged ash particles due to the charge on a particle alone or as a result of enhancement of the electric field on a particle in the presence of a net electric field caused by large-scale charge separation in the eruption column. These two possible mechanisms would not be exclusive and might be expected to occur at different stages in eruption column development or with some overlap. A particle that was sufficiently self-charged to produce corona without an external field might stop producing corona due to the corona itself (i.e., self-extinguishing) or due to aggregation with oppositely charged particles (James et al., 2002), which might explain why CRF does not tend to persist after an explosive event wanes. The rare cases where CRF was observed to be reduced in rate and amplitude following a relatively large lightning discharge when there was a net electrostatic field present is suggestive that some form of corona was occurring due to an external field; however, we note that this would not account for all the observations of CRF because CRF usually occurred when there was no net external field.

Our observations of the impulse duration of CRF events can provide an upper limit on the length scale of an individual CRF discharge. Rison et al. (2016) found the velocity of fast positive breakdown to be $3-7\times10^7$ m/s and that this velocity is altitude invariant. If we assume 7×10^7 m/s to be an upper limit on the possible speed of a CRF discharge, the observed duration of 160 ns gives an upper limit of 11.2 m on the length of CRF. In actuality this upper limit would be smaller, since the observed 160-ns duration includes ringing of the LMA band-pass filter. We estimate that the length of a CRF discharge would be a few meters at most.

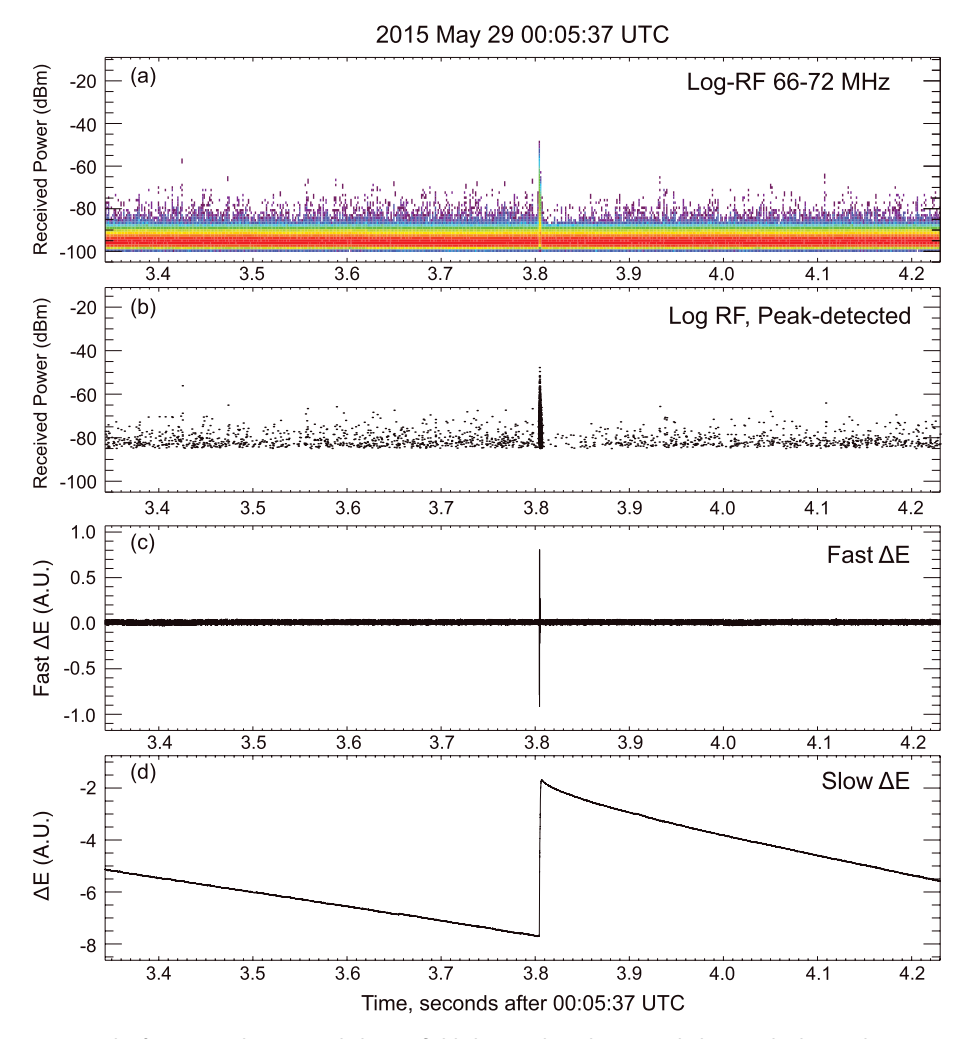


Figure 14. Log radio frequency (log-RF) and electric field change data showing a lightning discharge that occurred while continual radio frequency (CRF) was also occurring. A reduction in the rate and power of the CRF sources occurred immediately after the discharge at approximately 00:05:40.8. (a) Log-RF data; colors represent relative density of events with red being the highest density and blue the lowest density. (b) Peaks in the log-RF data, as determined by a peak detection algorithm. (c) Fast electric field change waveform. (d) Slow electric field change waveform.

4. Conclusions

Our observations offer evidence that the process producing CRF impulses is distinct from the process of forming lightning leaders. The most significant observation leading us to that conclusion is the log-RF data showing that an individual CRF impulse is a short impulse of at most 160 ns, while leader steps are composed of multiple subpulses. Further, the high-speed video observations showed that lightning discharges on the order of tens of meters in length were distinct from CRF; thus, we can revise the hypothesis put forth by Thomas et al. (2010) that CRF was produced by leader-forming discharges on the order of tens or a few hundreds of meters. We hypothesize that CRF is produced by a streamer discharge, or more generally a cold plasma discharge, as discussed above.

Though we have made progress on understanding the physical origin of CRF, we have not made any revision on the term used to describe the physical discharge process that produces CRF. The terms for the various types of electrical discharges that occur during volcanic eruptions were first outlined by Thomas et al. (2010) and were subsequently elaborated on by Behnke et al. (2013). These terms are vent discharge, "near-vent lightning," and "plume lightning." The word "discharge" was chosen for the first term because discharge is a general word lacking a precise definition within the field of lightning physics. One can use it to mean electrical discharge processes such as streamers (cold plasma) and leaders (hot plasma), while the term lightning



necessarily means a discharge involving leaders (Bazelyan & Raizer, 2000). Thus, the term vent discharge is purposefully vague, and it is still appropriate to use to describe the discharge that produces CRF. The evidence presented in this paper has given further insight into this discharge process, chiefly that a vent discharge is most likely a type of cold plasma discharge and thus is not lightning. We stress that a vent discharge is fundamentally distinct from near-vent lightning or plume lightning, which are both optically bright due to heating of the plasma channel. We expect vent discharges to be much less bright, so much so that they would be difficult to photograph, similar to a streamer discharge. Given this new understanding of vent discharges, we note that some authors' previous usage of the term vent discharge would now be considered inappropriate (e.g., Aizawa et al., 2016; Cimarelli et al., 2016); these authors were instead reporting on what we would most likely consider to be near-vent lightning, though there is room to refine the definitions of near-vent lightning and plume lightning as well. The current definition of near-vent lightning is a hot plasma discharge ranging in length from tens of meters to several kilometers that occurs relatively near the vent (Thomas et al., 2010). Plume lightning can also be relatively small (approximately a few hundreds of meters; Behnke et al., 2013) but are typically thought of as extensive lightning discharges (tens of kilometers in length) that occur due to large-scale charge separation in the plume, which results in horizontally stratified charge layers similar to that of thunderstorms (Thomas et al., 2010). The eruption of Redoubt Volcano and its profusion of lightning (Behnke et al., 2013) showed that defining the line between when and where near-vent lightning stops and plume lightning begins would be difficult. Such a definition may not serve much purpose anyway, but if there was one, its definition should rely on the physical characteristics of the discharge in addition to their placement and timing. The distinction between a vent discharge and a lightning discharge of any variety (e.g., near-vent or plume) is a much more important distinction.

These results further to our understanding of volcanic lightning and the electrical characteristics of volcanic plumes. CRF was detected before the eruption column rose above the crater rim and into the line of sight of the LMA sensors; thus, the volcanic ejecta were likely charged prior to exiting the vent (Smith et al., 2018). However, a net charge from the eruption column was not initially detected until a second or two after the onset of CRF; thus, there was not a significant imbalance in the quantity of positive or negative charge within the eruption column as it was initially ejected. Charge separation processes occurred subsequent to eruption. This also contradicts the conclusions drawn by Thomas et al. (2010), who surmised that the discharges producing CRF occurred because the eruption column natively carried a net charge.

These observations reinforce previous results showing that the CRF signal is an excellent indicator that an eruption is occurring (Behnke et al., 2013; Thomas et al., 2007, 2010). The observation that CRF was detected prior to the eruption column entering the line of sight of the LMA sensors shows that CRF was occurring while the eruption column was below the rim, and if it did not begin simultaneously with eruption, it began within milliseconds from eruption onset. The explosive events that produced CRF in this study are the smallest events from which CRF has been detected indicating that CRF detection may be a useful monitoring and research tool for even very small eruptions.

Acknowledgments

This research was supported by the National Science Foundation under grants AGS 1445704 and 1445703. Van Eaton acknowledges the U.S. Geological Survey Mendenhall Fellowship. We thank the Sakurajima Volcano Observatory for their support and use of their facilities and for assisting with LMA sensor siting. We particularly thank Masato Iguchi and Daisuke Miki for their efforts. The data presented here are archived on Zenodo with DOI: 10.5281/zenodo.1161235.

References

Aizawa, K., Cimarelli, C., Alatorre-Ibargüengoitia, M., Yokoo, A., Dingwell, D., & Iguchi, M. (2016). Physical properties of volcanic lightning: Constraints from magnetotelluric and video observations at Sakurajima volcano, Japan. *Earth and Planetary Science Letters*, 444, 44–55. Anderson, R., Björnsson, S., Blanchard, D., Gathman, S., Hughes, J., Jónasson, S., et al. (1965). Electricity in volcanic clouds. *Science*, 148(3674), 1179–1189.

Arason, P., Bennett, A., & Burgin, L. E. (2011). Charge mechanisms of volcanic lightning revealed during the 2010 eruption of Eyjafjallajökull. Journal of Geophysical Research, 116, B00C03. https://doi.org/10.1029/2011JB008651

Bazelyan, E., & Raizer, Y. (2000). Lightning physics and lightning protection. Philadephia: Institute of Physics Publishing.

Behnke, S. A., & McNutt, S. R. (2014). Using lightning observations as a volcanic eruption monitoring tool. *Bulletin of Volcanology*, *76*, 847. Behnke, S. A., Thomas, R. J., Edens, H. E., Krehbiel, P. R., & Rison, W. (2014). The 2010 eruption of Eyjafjallajökull: Lightning and plume charge structure. *Journal of Geophysical Research: Atmospheres*, *119*, 833–859. https://doi.org/10.1002/2013JD020781

Behnke, S. A., Thomas, R. J., Krehbiel, P. R., & McNutt, S. R. (2012). Spectacular lightning revealed in 2009 Mount Redoubt eruption. Eos Transactions American Geophysical Union, 93(20), 193.

Behnke, S. A., Thomas, R. J., McNutt, S. R., Schneider, D. J., Krehbiel, P. R., Rison, W., & Edens, H. E. (2013). Observations of volcanic lightning during the 2009 eruption of Redoubt Volcano. *Journal of Volcanology and Geothermal Research*, 259, 214–234. https://doi.org/10.1016/j.jvolgeores.2011.12.010

Bennett, A., Odams, P., Edwards, D., & Arason, P. (2010). Monitoring of lightning from the April–May 2010 Eyjafjallajökull volcanic eruption using a very low frequency lightning location network. *Environmental Research Letters*, 5(4), 44,013–44,022.

Brook, M., Moore, C., & Sigurgeirsson, T. (1974). Lightning in volcanic clouds. Journal of Geophysical Research, 79(3), 472 – 475.

Cimarelli, C., Alatorre-Ibargüengoitia, M., Aizawa, K., Yokoo, A., & Diaz-Marina, A. (2016). Multiparametric observations of volcanic lightning: Sakurajima volcano, Japan. *Geophysical Research Letters*, 43, 4221–4228. https://doi.org/10.1002/2015GL067445



- Cimarelli, C., Alatorre-Ibargüengoitia, M., Kueppers, U., Scheu, B., & Dingwell, D. (2014). Experimental generation of volcanic lightning. *Geology*, 42(1), 79–82. https://doi.org/10.1130/G34802.1
- Cooray, V., & Cooray, G. (2012). Electromagnetic radiation field of an electron avalanche. *Atmospheric Research*, 117, 18–27. https://doi.org/10.1016/j.atmosres.2011.06.004
- Dickinson, J. T., Langford, S. C., Jensen, L. C., McVay, G. L., Kelso, J. F., & Pantano, C. G. (1988). Fractoemission from fused silica and sodium silicate glasses. *Journal of Vacuum Science and Technology A*, 6, 1084–1089.
- Dürig, T., Gudmundsson, M. T., Karmann, S., Zimanowski, B., Dellino, P., Rietze, M., & Büttner, R. (2015). Mass eruption rates in pulsating eruptions estimated from video analysis of the gas thrust-buoyancy transition—A case study of the 2010 eruption of eyjafjallajökull, Iceland. *Earth. Planets and Space*. 67. 180.
- Gallimberti, I., Bacchiega, G., Bondiou-Clergerie, A., & Lalande, P. (2002). Fundamental processes in long air gap discharges. *Calum Raistrick Physique*, *3*, 1335–1359.
- Hamlin, T. (2004). The New Mexico Tech Lightning Mapping Array (PhD thesis). New Mexico Institute of Mining and Technology.
- Hill, J. D., Uman, M. A., & Jordan, D. M. (2011). High-speed video observations of a lightning stepped leader. *Journal of Geophysical Research*, 116. D16117. https://doi.org/10.1029/2011JD015818
- Hoblitt, R. (1994). An experiment to detect and locate lightning associated with eruptions of Redoubt Volcano. *Journal of Volcanology and Geothermal Research*, 62, 499–517.
- Houghton, I. M. P., Aplin, K. L., & Nicoll, K. A. (2013). Triboelectric charging of volcanic ash from the 2011 Grímsvötn eruption. *Physical Review Letters*, 111, 118501.
- James, M. R., Gilbert, J. S., & Lane, S. J. (2002). Experimental investigation of volcanic particle aggregation in the absence of a liquid phase. Journal of Geophysical Research, 107(B9), 2191. https://doi.org/10.1029/2001JB000950
- James, M. R., Lane, S. J., & Gilbert, J. S. (2000). Volcanic plume electrification Experimental investigation of fracture-charging mechanism. Journal of Geophysical Research, 105, 16,641 – 16,649.
- Mastin, L. G. (2007). A user-friendly one-dimensional model for wet volcanic plumes. *Geochemistry, Geophysics, Geosystems*, 8, Q03014. https://doi.org/10.1029/2006GC001455
- McNutt, S. R., & Davis, C. (2000). Lightning associated with the 1992 eruptions of Crater Peak, Mount Spurr Volcano, Alaska. *Journal of Volcanology and Geothermal Research*, 102, 45–65.
- McNutt, S. R., & Williams, E. (2010). Volcanic lightning: Global observations and constraints on source mechanisms. *Bulletin of Volcanolog*, 72(10), 1153—1167
- McNutt, S. R., Tytgat, G., Estes, S. A., & Stihler, S. D. (2010). A parametric study of the January 2006 explosive eruptions of Augustine Volcano, using seismic, infrasonic and lightning data. In J. Powers, M. Coombs, & J. Freymueller (Eds.), The 2006 eruption of Augustine Volcano, Alaska (pp. 86–102). U.S. Geological Survey Professional Paper 1769.
- Mendez Harper, J., & Dufek, J. (2016). The effects of dynamics on the triboelectrification of volcanic ash. *Journal of Geophysical Research: Atmospheres*, 121, 8209–8228. https://doi.org/10.1002/2015JD024275
- Miura, T., Koyaguchi, T., & Tanaka, Y. (2002). Measurements of electric charge distribution in volcanic plumes at Sakurajima Volcano, Japan. Bulletin of Volcanology, 64, 75–93.
- Rison, W., Krehbiel, P. R., Stock, M. G., Edens, H. E., Shao, X. M., Thomas, R. J., et al. (2016). Observations of narrow bipolar events reveal how lightning is initiated in thunderstorms. *Nature Communications*, 7, 10721. https://doi.org/10.1038/ncomms10721
- Rison, W., Thomas, R. J., Krehbiel, P. R., Hamlin, T., & Harlin, J. (1999). A GPS-based three-dimensional lightning mapping system—Initial observations. *Geophysical Research Letters*. 26, 3573–3576.
- Shao, X. M., & Krehbiel, P. R. (1996). The spatial and temporal development of intracloud lightning. *Journal of Geophysical Research*, 101(D21), 26.641–26.668
- Smith, C. M., Van Eaton, A. R., Charbonniera, S., McNutta, S. R., Behnke, S. A., Thomas, R. J., et al. (2018). Correlating the electrification of volcanic plumes with ashfall textures at Sakurajima Volcano, Japan. *Earth and Planetary Science Letters*, 492, 47–58. https://doi.org/10.1016/j.epsl.2018.03.052
- Thomas, R. J., Krehbiel, P. R., Rison, W., Edens, H. E., Aulich, G. D., Winn, W. P., et al. (2007). Electrical activity during the 2006 Mount St. Augustine volcanic eruptions. *Science*, *315*, 1097.
- Thomas, R. J., Krehbiel, P. R., Rison, W., Hunyady, S., Winn, W. P., Hamlin, T., & Harlin, J. (2004). Accuracy of the Lightning Mapping Array. Journal of Geophysical Research, 109, D14207. https://doi.org/10.1029/2004JD004549
- Thomas, R. J., McNutt, S. R., Krehbiel, P. R., Rison, W., Aulich, G., Edens, H. E., et al. (2010). Lightning and electrical activity during the 2006 eruption of Augustine Volcano. In J. Powers, M. Coombs, & J. Freymueller (Eds.), *The 2006 eruption of Augustine Volcano, Alaska* (pp. 579–608). U.S. Geological Survey Professional Paper 1769.
- Valade, S. A., Harris, A. J. L., & Cerminara, M. (2014). Plume ascent tracker: Interactive Matlab software for analysis of ascending plumes in image data. *Computers and Geosciences*, 66, 132–144. https://doi.org/10.1016/j.cageo.2013.12.015
- Van Eaton, A. R., Amigo, A., Bertin, D., Mastin, L. G., Giacosa, R. E., Gonzalez, J., et al. (2016). Volcanic lightning and plume dynamics reveal evolving hazards during the April 2015 eruption of Calbuco volcano, Chile. *Geophysical Research Letters*, 43, 3563–3571. https://doi.org/10.1002/2016GL068076
- Winn, W. P., Aulich, G. D., Hunyady, S. J., Eack, K. B., Edens, H. E., Krehbiel, P. R., et al. (2011). Lightning leader stepping, K changes, and other observations near an intracloud flash. *Journal of Geophysical Research*, 116, D23115. https://doi.org/10.1029/2011JD015998
- Wu, T., Wang, D., Rison, W., Thomas, R. J., Edens, H. E., Takagi, N., & Krehbiel, P. R. (2017). Corona discharges from a windmill and its lightning protection tower in winter thunderstorms. *Journal of Geophysical Research: Atmospheres*, 122, 4849–4865. https://doi.org/10.1002/2016JD025832